

SU(4) Kondo Effect in Carbon Nanotubes

Manh-Soo Choi,¹ Rosa López,² and Ramón Aguado³

¹*Department of Physics, Korea University, Seoul 136-701, Korea*

²*Département de Physique Théorique, Université de Genève, CH-1211 Genève 4, Switzerland*

³*Teoría de la Materia Condensada, Instituto de Ciencia de Materiales de Madrid (CSIC) Cantoblanco, 28049 Madrid, Spain*
(Dated: November 12, 2018)

We investigate theoretically the non-equilibrium transport properties of carbon nanotube quantum dots. Owing to the two-dimensional band structure of graphene, a double orbital degeneracy plays the role of a pseudo-spin, which is entangled with the spin. Quantum fluctuations between these four degrees of freedom result in an SU(4) Kondo effect at low temperatures. This exotic Kondo effect manifests as a four-peak splitting in the non-linear conductance when an axial magnetic field is applied.

PACS numbers: 75.20.Hr, 73.63.Fg, 72.15.Qm

Introduction.— Carbon nanotubes (CNTs) exhibit a good deal of remarkable transport phenomena including quantum interference [1], Luttinger liquid features [2] or spin polarized transport [3]. Finite-length CNTs behave like quantum dots (QDs) and thus show Coulomb blockade [4, 5] and Kondo physics [6]. Interestingly, the richness of the band structure of CNTs and the feasibility to attach new materials as electrodes, e.g., ferromagnetic [3] or superconducting contacts [7], allows us to explore new aspects of the Kondo effect, one of the most fundamental topics in condensed matter physics.

The electronic states of a CNT form one-dimensional electron and hole sub-bands. They originate from the quantization of the electron wavenumber perpendicular to the nanotube axis, k_{\perp} , which arises when graphene is wrapped into a cylinder to create a CNT. By symmetry, for a given sub-band at $k_{\perp} = k_0$ there is a second degenerate sub-band at $k_{\perp} = -k_0$. Semiclassically, this degeneracy corresponds to the clockwise (\odot) or counter-clockwise (\ominus) symmetry of the wrapping modes. Linear transport measurements in the Coulomb blockade regime reveal a distinct four-fold shell filling pattern owing to the orbital and the spin degeneracies [5].

In this Letter we combine several theoretical approaches, scaling theory, numerical renormalization group (NRG) [8], non-crossing approximation (NCA) [9], equation-of-motion (EOM) [10] methods, to present a unified picture of low-temperature, non-equilibrium transport through CNT quantum dots in the presence of magnetic fields. We show that quantum fluctuations between the four states $\{\odot\uparrow, \odot\downarrow, \ominus\uparrow, \ominus\downarrow\}$ may dominate transport at low temperatures provided that both the orbital and spin indexes are conserved during tunneling. This leads to a highly symmetric SU(4) Kondo effect, and hence an enhanced Kondo temperature, in which the spin and the orbital degrees of freedom are totally entangled [11]. We also point out that the orbital degeneracy in the dot itself is not enough for having SU(4) Kondo physics. In general, SU(2) Kondo physics is possible. We show that neither an enhanced Kondo temperature nor linear

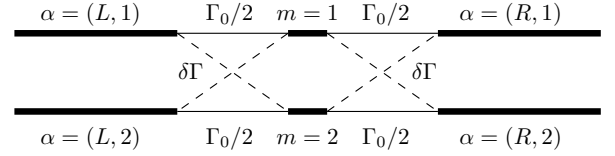


FIG. 1: A schematic of couplings between the degenerate orbitals $[m = 1(2)]$ with conduction channels $[L(R), m]$.

conductance measurements can distinguish between the two effects. Instead, the non-linear conductance in the presence of a *parallel* magnetic field shows a four-peak structure, with different splittings for the spin and the orbital sectors, which unambiguously signals SU(4) Kondo physics. Our theoretical results are in good agreement with recent experiments by Jarillo-Herrero *et al* [12].

Model.— We study a quantum dot CNT coupled to left (L) and right (R) electrodes. We consider the case where the QD has two (nearly) degenerate localized orbitals [labeled by the quantum number $m = 1, 2$ where 1(2) denotes \odot (\ominus) orbital mode, respectively]. The presence of an axial magnetic field (B_{\parallel}) lifts *both* the orbital and spin degeneracies: A parallel magnetic field induces an Aharonov-Bohm phase $2\pi\Phi/\Phi_0$, where $\Phi = \pi d_t^2/4B_{\parallel}$ is the flux threading the nanotube, $\Phi_0 = h/e$ is the flux quantum and d_t the tube diameter. This Aharonov-Bohm flux shifts the allowed k_{\perp} and the orbital degeneracy is lifted by an amount $\pm\Delta_{\text{orb}} = \pm ed_t v_F B_{\parallel}/4$, where v_F is the Fermi velocity [13]. The states near the energy gap correspond to semiclassical orbits which have an *orbital* magnetic moment $\mu_{\text{orb}} = ed_t v_F/4$. Thus, an axial magnetic field leads to an energy shift $\Delta_{\text{orb}} = \mu_{\text{orb}} B_{\parallel}$. The states further split due to the Zeeman energy $\pm\Delta_Z/2 = \pm g\mu_B B_{\parallel}/2$, where μ_B is the Bohr magneton and $g \approx 2$ is the g -factor in nanotubes. μ_{orb} scales with the CNT diameter and is typically one order of magnitude larger than the Bohr magneton [12, 14] resulting in a stronger influence of B_{\parallel} on the orbital sector. Thus, the single particle energy $\epsilon_{m\sigma}$ associ-

ated with the orbital m and the spin σ is given by: $\epsilon_{m\sigma} = \epsilon_d + \Delta_{\text{orb}}(\delta_{m,1} - \delta_{m,2}) + (\Delta_Z/2)(\delta_{\sigma,\uparrow} - \delta_{\sigma,\downarrow})$. The QD is then described by the Hamiltonian

$$\mathcal{H}_D = \sum_{m=1,2} \sum_{\sigma=\uparrow,\downarrow} \epsilon_{m,\sigma} d_{m,\sigma}^\dagger d_{m,\sigma} + \frac{1}{2} U(n - n_g)^2, \quad (1)$$

where $n = \sum_{m,\sigma} d_{m,\sigma}^\dagger d_{m,\sigma}$ is the occupation and U is the Hubbard-like on-site interaction (we focus on the regime where the QD is occupied by a single electron). The two leads are modelled as:

$$\mathcal{H}_C = \sum_{\alpha \in L, R} \sum_{m=1,2} \sum_{k,\sigma} \epsilon_{\alpha,k} c_{\alpha,k,m,\sigma}^\dagger c_{\alpha,k,m,\sigma}, \quad (2)$$

Without loss of generality, we assume that there are two distinguished (groups of) channels $m = 1, 2$ in each lead. The coupling between the leads and the dot is described by the tunneling Hamiltonian of the following form

$$\mathcal{H}_T = \sum_{\alpha,k,\sigma} \sum_{m,m'} V_{m,m'}^\alpha \left(c_{\alpha,k,m,\sigma}^\dagger d_{m',\sigma} + h.c. \right), \quad (3)$$

where the tunneling amplitudes read $V_{m,m'}^\alpha = [V_0 \delta_{m,m'} + V_X(1 - \delta_{m,m'})]/\sqrt{2}$, (for simplicity, we ignore the k - and σ -dependence of the tunneling amplitudes). In the most general case, they describe two types of tunneling processes (see Fig. 1): (i) those in which the orbital quantum number is conserved, denoted by $V_{1,1}^\alpha = V_{2,2}^\alpha = V_0/\sqrt{2}$ and (ii) those events accounting for mixing (cross coupling) $V_{m,m'}^\alpha = V_X/\sqrt{2}$ with $m \neq m'$. To gain more physical intuition when $V_X \neq 0$ we rewrite the total Hamiltonian $\mathcal{H} = \mathcal{H}_D + \mathcal{H}_C + \mathcal{H}_T$ in terms of symmetric (even) and antisymmetric (odd) combinations of the orbital channels. Before, we simplify the algebra by performing a canonical transformation, $c_{L(R),k,m,\sigma} = (a_{k,m,\sigma} \pm b_{k,m,\sigma})/\sqrt{2}$, such that the resulting Hamiltonian contains only a single lead, $a_{k,m,\sigma} = (c_{L,k,m,\sigma} + c_{R,k,m,\sigma})/\sqrt{2}$, with two channels $m = 1, 2$. Next, we apply the even-odd transformation $a_{k,1(2),\sigma} = (c_{k_e\sigma} \pm i c_{k_o\sigma})/\sqrt{2}$ and $d_{1(2)\sigma} = (d_{e\sigma} \pm i d_{o\sigma})/\sqrt{2}$, such that \mathcal{H} reads,

$$\begin{aligned} \mathcal{H} = & \sum_{\sigma,\nu=e,o} \epsilon_{k\nu} c_{k\nu,\sigma}^\dagger c_{k\nu,\sigma} + \sum_{\sigma,\nu=e,o} \epsilon_{\nu\sigma} d_{\nu,\sigma}^\dagger d_{\nu,\sigma} + U(n - n_g) \\ & + V^e \sum_{k_e,\sigma} \left(c_{k_e,\sigma}^\dagger d_{e\sigma} + h.c. \right) + V^o \sum_{k_o,\sigma} \left(c_{k_o,\sigma}^\dagger d_{o\sigma} + h.c. \right), \end{aligned} \quad (4)$$

with $V^e \equiv V_0 + V_X$ and $V^o \equiv V_0 - V_X$ (note that $\epsilon_{k\nu}$ and $\epsilon_{\nu\sigma}$ remain invariant under this transformation). In the absence of cross coupling terms $V_X = 0$ both, the even and odd orbitals are equally coupled to the QD ($V^e = V^o = V_0$). Thus, at small energies the effective model leads to SU(4) Kondo physics, see below. However, for the maximal mixing, i.e. $V_X = V_0$, the even orbital is doubly coupled to the dot ($V^e = 2V_0$) whereas the

odd orbital becomes *uncoupled* ($V^o = 0$). Here, SU(2) Kondo physics arises owing to spin fluctuations in the even orbital channel.

Effective Kondo model.—Let us now substantiate our previous arguments by examining the low-energy properties of the system. After performing a Schrieffer-Wolf transformation to \mathcal{H} the effective Hamiltonian reads:

$$\begin{aligned} \mathcal{H}_K = & \mathcal{H}_C + \frac{J_1}{4} [\mathbf{S} \cdot (\psi^\dagger \boldsymbol{\sigma} \psi) + \mathbf{S} \cdot (\psi^\dagger \boldsymbol{\sigma} \tau^z \psi) T^x] \\ & + \frac{J_2}{4} [\mathbf{S} \cdot (\psi^\dagger \boldsymbol{\sigma} \tau^\perp \psi) \cdot \mathbf{T}^\perp + (\psi^\dagger \boldsymbol{\tau}^\perp \psi) \cdot \mathbf{T}^\perp] \\ & + \frac{J_3}{4} (\psi^\dagger \tau^z \psi) T^x + \frac{J_4}{4} [\mathbf{S} \cdot (\psi^\dagger \boldsymbol{\sigma} \tau^z \psi) + \mathbf{S} \cdot (\psi^\dagger \boldsymbol{\sigma} \psi) T^x] \\ & - J_5 T^x + \mu_B g \mathbf{B} \cdot \mathbf{S} + \mu_{\text{orb}} \mathbf{B} \cdot \mathbf{T}, \end{aligned} \quad (5)$$

where $\psi_k^\dagger = [c_{e,k,\uparrow}^\dagger, c_{e,k,\downarrow}^\dagger, c_{o,k,\uparrow}^\dagger, c_{o,k,\downarrow}^\dagger]$ are the field operators for the leads in the even-odd basis and $\psi = \sum_k \psi_k$. The field operator for the QD $\psi_d^\dagger = [d_{e,\uparrow}^\dagger, d_{e,\downarrow}^\dagger, d_{o,\uparrow}^\dagger, d_{o,\downarrow}^\dagger]$ defines the orbital pseudo-spin and the spin operators given by $\mathbf{T} = \psi_d^\dagger \boldsymbol{\tau} \psi_d$ and $\mathbf{S} = \psi_d^\dagger \boldsymbol{\sigma} \psi_d$ respectively, with τ and σ being the Pauli matrices in the orbital pseudo-spin and spin spaces, respectively. Here, $T^\perp (\tau^\perp)$ denotes $T^y + T^z (\tau^y + \tau^z)$. Using renormalization group (RG) arguments, the effective coupling constants in the U -large limit are given initially by $J_1 = J_3 = \mathcal{N} V^2 / \epsilon_d$, $J_2 = J_1 (|V_0|^2 - |V_X|^2) / V^2$, $J_4 = J_1 |2V_0 V_X| / V^2$, where $V^2 = |V_0|^2 + |V_X|^2$ (\mathcal{N} is the degeneracy). J_5 is not renormalized in the RG procedure and does not flow into the strong coupling regime. At zero magnetic field with only spin and orbital conserving tunneling processes ($V_X = 0$), $J_1 = J_2 = J_3 = J$ while $J_4 = J_5 = 0$. The corresponding Hamiltonian is reduced to the SU($\mathcal{N}=4$) Kondo model where the spin \mathbf{S} and the orbital pseudo-spin \mathbf{T} are entangled (last term of the equation),

$$\mathcal{H}_{\text{SU}(4)} = \mathcal{H}_C + (J/4) [\mathbf{S} \cdot (\psi^\dagger \boldsymbol{\sigma} \psi) + (\psi^\dagger \boldsymbol{\tau} \psi) \cdot \mathbf{T} + \mathbf{S} \cdot (\psi^\dagger \boldsymbol{\sigma} \boldsymbol{\tau} \psi) \cdot \mathbf{T}]. \quad (6)$$

The scaling equations are reduced to a single equation

$$dJ / \ln D = \mathcal{N} \rho_0 J^2, \quad (7)$$

where ρ_0 is the density of states (DOS) in the leads and D is the bandwidth, resulting in the exponentially enhanced Kondo temperature $T_K^{\text{SU}(4)} \approx D \exp[1/(\mathcal{N} \rho_0 J)]$ compared with $T_K^{\text{SU}(2)}$ of the single-level SU($\mathcal{N}=2$) model.

In the other limiting case ($V_X = V_0$), the corresponding Kondo-like Hamiltonian [Eq. (5) at $B = 0$ with $J_1 = J_3 = J_4 = 2\mathcal{N}|V_0|^2/\epsilon_d$ and $J_2 = 0$] involves only spin fluctuations in the doubly degenerate ($\mathcal{N}=2$) even orbital. It gives rise to what we call a two-level (TL) SU(2) model: $\mathcal{H}_{\text{TL SU}(2)} = \mathcal{H}_C + J \mathbf{S}_e \cdot (\psi_e^\dagger \boldsymbol{\sigma} \psi_e) (1 + T^x) + (J/4) (\psi_e^\dagger \psi_e) T^x - J_5 T^x$. The RG equation for J is

$$dJ / \ln D = 2\mathcal{N} \rho_0 J^2. \quad (8)$$

This model corresponds to an SU(2) Fermi liquid [15] with a Kondo temperature $T_K^{\text{TLSU}(2)}$ which is the same as $T_K^{\text{SU}(4)}$ (compare Eqs. (7) and (8), the factor 2 comes from the doubling of the coupling $2V_0$ [16]).

The scaling arguments above are confirmed by the NRG studies of the spectral density $A_{m\sigma}(\omega)$ for the localized level $m\sigma$. At $B_{\parallel} = 0$, the spectral density shows a peak near the Fermi energy, corresponding to the formation of the SU(4) Kondo state; see Fig. 2 (solid line in the right inset). The peak width, which is much broader than that for the SU(2) Kondo model (dotted line), demonstrates the exponential enhancement of the Kondo temperature mentioned above. Another remarkable effect is that the SU(4) Kondo peak shifts away from $\omega = E_F = 0$ and is pinned at $\omega \approx T_K^{\text{SU}(4)}$. This can be understood from the Friedel sum rule [17] which, in this case, gives $\delta = \pi/4$ for the scattering phase shift at E_F . Accordingly, the linear conductance at zero temperature is given by $\mathcal{G}_0 = 4(e^2/h)\sin^2\delta = 2e^2/h$. It is interesting to recall that the Friedel sum rule gives the same linear conductance also for the TL SU(2) Kondo model. Thus, neither the enhancement of the Kondo temperature nor the linear conductance, can distinguish between the SU(4) and the TL SU(2) Kondo effects. This can only be achieved by studying the influence of a parallel magnetic field, which we do now.

SU(4) Kondo model at finite field.— Because of the underlying SU(4) symmetry, the orbital pseudo-spin should behave the same way as the real spin. In particular, the lift of the pseudo-spin degeneracy will split the Kondo peak (as long as the lift is larger than the Kondo temperature) just like the Zeeman splitting of the real spin does. The only difference is that pseudo-spin is more susceptible to the magnetic field than the real spin since $\mu_{\text{orb}} \gg \mu_B$ (see above). Therefore, at sufficiently large fields ($2\Delta_{\text{orb}} \gg \Delta_Z \gg T_K^{\text{SU}(4)}$), one has four split-Kondo peaks at $\omega \approx \pm 2\Delta_{\text{orb}}$ and $\omega \approx \pm \Delta_Z$; see Fig. 2 (left inset). At moderate fields such that $2\Delta_{\text{orb}} \gtrsim T_K^{\text{SU}(4)} \gg T_K^{\text{SU}(2)} \gtrsim \Delta_Z$, one can have a three-peak structure; see Fig. 2 (dashed line). The lifted degeneracy in the orbital pseudo-spin gives two side-peaks at $\omega \approx \pm 2\Delta_{\text{orb}}$ while the spin still retains a Kondo effect and gives the central peak. The central peak (which is now at $\omega = 0$) corresponds to a conventional SU(2) Kondo effect and hence is much narrower than the central resonance for $B_{\parallel} = 0$.

The above features of $A_{\text{tot}}(\omega)$ at equilibrium are directly reflected in the non-linear conductance, $\mathcal{G} \equiv dI/dV$, an experimentally measurable quantity. The current through the system I can be expressed in terms of the local DOS [18]: $I = (e/h) \sum_{\sigma=\uparrow,\downarrow} \sum_{m=1,2} \int d\omega [f_L(\omega) - f_R(\omega)] [\Gamma_0(\omega) + \delta\Gamma(\omega)] A_{m\sigma}(\omega)$, where $\Gamma_0(\omega) = \pi\rho_0(\omega)|V_0|^2$, $\delta\Gamma(\omega) = \pi\rho_0(\omega)|V_X|^2$, and $f_{L(R)}$ is the Fermi function for the left(right) lead. The NRG procedure is valid only at equi-

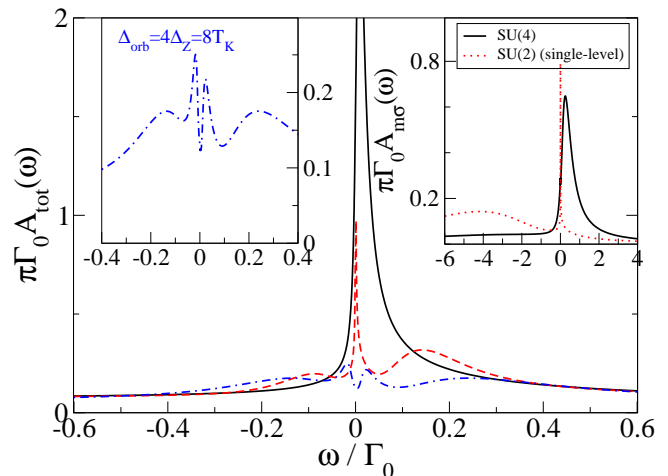


FIG. 2: (Color online) NRG results for the total spectral density $A_{\text{tot}}(\omega)$. The solid line is for the case of $\Delta_{\text{orb}} = \Delta_Z = 0$, the dashed line for $\Delta_{\text{orb}} = 8T_K^{\text{SU}(4)}$ ($T_K^{\text{SU}(4)} = 0.0133\Gamma_0$) with $\Delta_Z \approx 0$, and the dash-dotted line for $\Delta_{\text{orb}} = 4\Delta_Z = 8T_K^{\text{SU}(4)}$. (Parameters: $\epsilon_d = -10\Gamma_0$, $U = 200\Gamma_0$, $\Gamma_0 = 0.01D$, and $\delta\Gamma = 0$). Left inset: Zoom of the four peak splitting in $A_{\text{tot}}(\omega)$. Right inset: Comparison of the SU(4) (solid line) and the single-level SU(2) (dotted line) Kondo models. (Parameters: $\epsilon_d = -5\Gamma_0$, $U = 500\Gamma_0$, $\Gamma_0 = 0.02D$, and $\delta\Gamma = 0$).

librium so we need a method capable to produce the non-equilibrium DOS and the non-linear current. We choose to use a combination of the NCA and the EOM methods [10]. Figures 3(a) and (b) display the local DOS and the differential conductance, respectively, for several B_{\parallel} . We take Δ_{orb} ranging from $\Delta_{\text{orb}} = 0.5T_K^{\text{SU}(4)}$ to $\Delta_{\text{orb}} = 1.5T_K^{\text{SU}(4)}$ with $\mu_{\text{orb}} = 10\mu_B$ leading to $\Delta_Z = \Delta_{\text{orb}}/5$. For the lowest magnetic field, $A_{\text{tot}}(\omega)$ exhibits two splittings, namely the orbital and the Zeeman splittings with peaks at $\omega \approx \pm 2\Delta_{\text{orb}}$ and $\omega \approx \pm \Delta_Z$, respectively, in excellent agreement with the NRG calculations. As Δ_{orb} enhances beyond, a substructure arises in the outer peaks. These new side-peaks at $\omega \approx \pm 2\Delta_{\text{orb}} \pm \Delta_Z$ correspond to the simultaneous *spin-flip inter-orbital* transitions. Increasing further B_{\parallel} these side-peaks in the DOS get better resolved [19]. All these features are also present in the differential conductance plotted in Fig. 3(b).

Two-level SU(2) Kondo model at finite field.—As already shown, both the SU(4) and TL SU(2) Kondo models lead to similar results for the Kondo temperature and the linear conductance. Nevertheless, the inherent physics is completely different. In the highly symmetric SU(4) Kondo model, the orbital pseudo-spin and the real spin are indistinguishable (and screened simultaneously at zero field). On the contrary, in less symmetric multiple-level SU(2) Kondo models, the spin should be clearly distinguished from the orbital sector (tunneling processes preserve *only the spin*). This becomes clear at finite magnetic fields: When B_{\parallel} lifts the orbital degener-

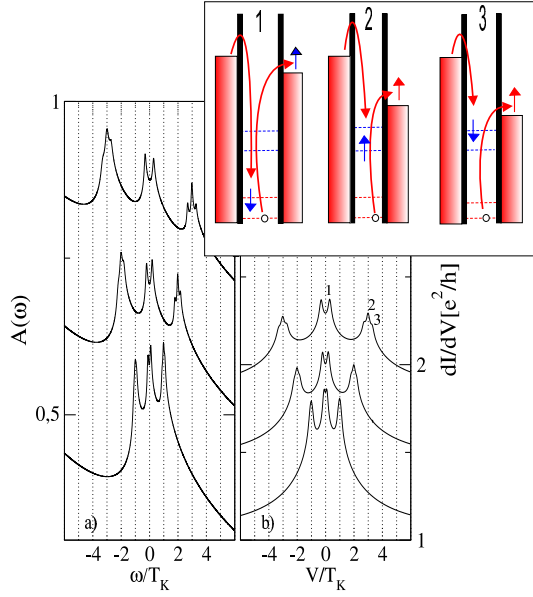


FIG. 3: (Color online). *NCA+EOM results for the SU(4) Kondo model.* (a) $A_{\text{tot}}(\omega)$ and (b) dI/dV versus eV for different magnetic fields ranging from $\Delta_{\text{orb}} = 0.5T_K^{\text{SU}(4)}$ (bottom) to $\Delta_{\text{orb}} = 1.5T_K^{\text{SU}(4)}$ (top). (The curves are shifted vertically for clarity). When $B_{\parallel} \neq 0$, the Kondo resonance splits due to the removal of both spin and orbital degeneracies. The rest of parameters are: $\epsilon_d = -4\Gamma_0$ and $T = 0.003\Gamma_0$ with $\delta\Gamma = 0$. The quantum dot is symmetrically coupled to two leads ($\Gamma_L = \Gamma_R = \Gamma_0$) consisting of Lorentzian bands of width $2D = 20\Gamma_0$. Inset: schematic representation of the allowed transitions. 1) intra-orbital *with spin-flip*, 2) inter-orbital *without spin-flip* and 3) inter-orbital *with spin-flip*.

acy, only the lower orbital level is occupied so the physics is essentially that of a single level Kondo model [16]. The Kondo resonance peak gets narrower with increasing B_{\parallel} . Since B_{\parallel} also breaks the spin degeneracy, the resulting DOS displays the usual Zeeman splitting. Overall, there are only two peaks around E_F (Fig. 4).

Summary.— We have demonstrated that quantum fluctuations between the orbital and the spin degrees of freedom in carbon nanotube QDs result in an SU(4) Kondo effect at low temperatures. This exotic Kondo effect manifests as a four-peak splitting in the non-linear conductance when an axial magnetic field is applied. Similar effects may appear in other systems like vertical dots [20] where the orbital quantum number is preserved during tunneling. Recent transport experiments in CNTs [12] clearly support our theoretical findings.

We thank Pablo Jarillo-Herrero, Silvano de Franceschi and Leo Kouwenhoven for sharing their experimental results with us prior to publication and for many helpful discussions. We also thank Markus Büttiker, Karyn Le Hur and David Sánchez for fruitful discussions. Work supported by the EU RTN No.HPRN-CT-2000-00144, the Spanish MECD and MCyT through grant MAT2002-

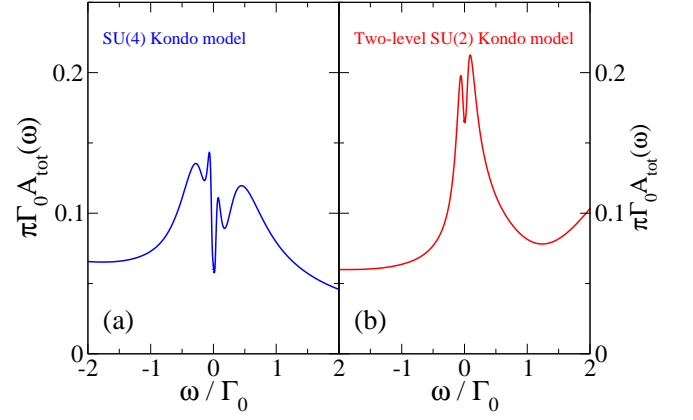


FIG. 4: (Color online). NRG results for the total spectral density comparing (a) the SU(4) Kondo model ($\delta\Gamma = 0$) and (b) the two-level SU(2) Kondo model ($\delta\Gamma = \Gamma_0$). Parameters are $\Delta_{\text{orb}} = 5\Delta_Z = 15T_K^{\text{SU}(4)} (\approx 0.2\Gamma_0)$, $\epsilon_d = -10\Gamma_0$, $U = 1000\Gamma_0$, and $\Gamma_0 = 0.01D$.

02465 and the "Ramón y Cajal" program, the SKORE-A, and the eSSC at Postech.

-
- [1] W. Liang *et al.*, Nature (London) **411**, 665 (2001).
 - [2] M. Bockrath *et al.*, Nature (London) **397**, 598 (1999).
 - [3] K. Tsukagoshi, B.W. Alphenaar, and H. Ago Nature (London) **401**, 572 (1999).
 - [4] M. Bockrath *et al.*, Science **275**, 1922 (1997). S.J. Tans *et al.*, Nature (London) **394**, 761 (1998).
 - [5] Wenjie Liang *et al.*, Phys. Rev. Lett. **88**, 126801 (2002); M.R. Buitelaar *et al.*, Phys. Rev. Lett. **88**, 156801 (2002).
 - [6] J. Nygård, D.H. Cobden, and P.E. Lindelof, Nature (London) **408**, 342 (2000). W. Liang *et al.*, *ibid* **417**, 725 (2002).
 - [7] M.R. Buitelaar *et al.*, Phys. Rev. Lett. **89**, 256801 (2002); M.R. Gräber *et al* cond-mat/0406638 (unpublished) (2004).
 - [8] K. G. Wilson, Rev. Mod. Phys. **47**, 773 (1975).
 - [9] D.C. Langreth and P. Nordlander, Phys. Rev. B **43**, 2541 (1991). N.S. Wingreen and Y. Meir, Phys. Rev. B **49**, 11 040 (1994). M.H. Hettler, J. Kroha, and S. Hershfield, Phys. Rev. B **58**, 5649 (1998).
 - [10] We combine occupations obtained from a non-equilibrium $U \rightarrow \infty$ NCA calculation with EOM retarded Greens function and include the finite lifetime of the intermediate states due to cotunneling at finite voltages and/or magnetic fields. See, Y. Meir, N.S. Wingreen, and P. A. Lee, Phys. Rev. Lett. **70**, 2601 (1993).
 - [11] Other device geometries have been recently proposed to obtain SU(4) Kondo effect in quantum dots. See, L. Borda *et al.*, Phys. Rev. Lett. **90**, 026602 (2003); K. Le Hur and P. Simon Phys. Rev. B **67**, 201308(R) (2003); G. Zaránd *et al.*, Solid State Commun. **126**, 463 (2003); R. López *et al.*, cond-mat/0402361 (unpublished) (2004).
 - [12] P. Jarillo-Herrero *et al.*, to be published (2004).
 - [13] H. Ajiki and T. Ando, Journal of the Phys. Soc. Jap. **62** 1255 (1993).

- [14] E.D. Minot *et al.*, Nature (London) **428**, 536 (2004).
- [15] G. Zarand Phys. Rev. B **52**, 13 459 (1995).
- [16] See also, D. Boese, W. Hofstetter, and H. Schoeller, Phys. Rev. B **66**, 125315 (2002).
- [17] D.C. Langreth, Phys. Rev. **150**, 516 (1966).
- [18] Y. Meir and N. S. Wingreen, Phys. Rev. Lett. **68**, 2512 (1992).
- [19] The NRG calculations in equilibrium also show a tiny substructure around the $\omega \approx \pm 2\Delta_{\text{orb}} \pm \Delta_Z$ indicating the occurrence of spin-flip inter-orbital transitions. However, due to the broadening of the outer peaks we are not able to resolve the peaks inside.
- [20] S. Sasaki *et al.*, Phys. Rev. Lett. **93**, 017205 (2004). In this experiment only two peaks, located at $\omega \approx \pm 2\Delta_{\text{orb}}$, are resolved in the dI/dV as the orbital degeneracy is lifted. No signatures of conventional $S = 1/2$ spin Kondo physics are resolved (probably because $T > T_K^{\text{SU}(2)}$).